Inorganic Chemistry

Article

pubs.acs.org/IC

# Effects of Te(IV) Oxo-Anion Incorporation into Thorium Molybdates and Tungstates

Bin Xiao,[†,‡] Martina Klinkenberg,[†] Dirk Bosbach,[†] Evgeny V. Suleimanov,[§] and Evgeny V. Alekseev*[,†,‡]

[†]Institute of Energy and Climate Research (IEK-6), Forschungszentrum Jülich GmbH, 52428 Jülich, Germany

[‡]Institut für Kristallographie, RWTH Aachen University, 52066 Aachen, Germany

[§]Department of Chemistry, Lobachevsky State University of Nizhny Novgorod, 603950 Nizhny Novgorod, Russia

Supporting Information

**ABSTRACT:** The exploration of phase formation in the Th−Mo/W−Te systems has resulted in four mixed oxo-anion compounds from high-temperature solid-state reactions: $ThWTe_2O_9$, $Th(WO_4)(TeO_3)$, $ThMoTe_2O_9$, and $Th_2(MoO_4)(TeO_3)_3$. All four compounds contain edge-sharing thorium polyhedra linked by $MoO_4/WO_6$ and different tellurium oxo-groups to form three-dimensional frameworks. In $ThWTe_2O_9$, each helical Th based chain is connected by four tungstotellurite clusters resulting in a building fragment which has a cross-section of four-leafed clovers. The structure of $Th(WO_4)(TeO_3)$ exhibits a multilayer-sandwich framework composed of thorium tellurite layers with tungsten chains in between. In the case of the molybdate family, $ThMoTe_2O_9$ and $Th_2(MoO_4)(TeO_3)_3$ are built from puckered Th−Te sheets which are further interconnected by $MoO_4$ tetrahedral linkers. The DSC-TG technique was performed to gain insight into the thermal behavior of the synthesized compounds. Raman spectra of as-prepared phases were obtained and analyzed for signature peaks.

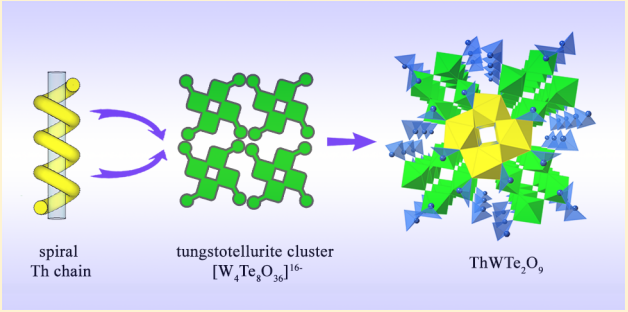


## 1. INTRODUCTION

The solid-state chemistry of actinides has been widely noted and studied in recent years, not only because of its significant relevance to nuclear waste management, but also because of exceedingly rich topological structural types and electronic properties of solid state actinide compounds.[1−4] The diverse structural chemistry of actinides is partly due to the unique coordination geometries and the different oxidation states of actinide centers. Actinides in higher oxidation states (5+, 6+, and 7+) typically form an approximately linear actinyl cation ($AnO_2^{2+}$), which can link with four to six donor atoms in its equatorial plane leading to tetrahedral, pentagonal, or hexagonal bipyramidal configurations.[5] In contrast, actinides in lower oxidation states (2+, 3+, and 4+) are usually found to result in a more complex geometry with the ability to achieve high coordination numbers.[6] Thorium, for instance, in a normal case is fixed to 4+ and can coordinate with up to 15 ligands to result in fascinating topological geometries and properties.[7] For example, $[ThB_5O_6(OH)_6][BO(OH)_2]\cdot 2.5H_2O$ (NDTB-1), as a notable representative, encompasses a supertetrahedral cationic framework, presenting a remarkable anion exchange capability that is particularly highlighted by selectively removing $TcO_4^-$ from nuclear waste streams.[8−10] Additionally, due to its stability in the tetravalent state, Th(IV) is frequently used as an ideal structural surrogate for studying other actinides (IV), especially those with high handling issues such as Np(IV) and Pu(IV).[11,12]

In the midst of numerous actinide compounds, one of the poorly investigated families is the actinide tellurites. It is also the case for thorium where phosphate,[13,14] molybdate,[15,16] and silicate[17] compounds have been mostly been studied. The actinide tellurite family was first encountered from a handful of minerals including cliffordite ($UO_2(Te_3O_7)$),[18] moctezumite ($PbUO_2(TeO_3)_2$),[19] and schmitterite ($UO_2(TeO_3)$).[20] The structural chemistry of $Te^{4+}$ is remarkably rich. Unlike $Se^{4+}$ which mainly exists in trigonal pyramidal $SeO_3$, $Te^{4+}$ can exist in diverse coordination geometries, such as $TeO_3$ trigonal pyramidal, $TeO_4$ disphenoid, and $TeO_5$ square pyramidal.[21,22] Moreover, these units can be further interconnected by corner-sharing to create complex tellurium polymers, leading to clusters, one-dimensional chains, two-dimensional sheets, and three-dimensional framework structural types.[23−25] $NH_4ATe_4O_9\cdot 2H_2O$ (A = Rb or Cs) is a rare example in which three types of tellurium polyhedral coordination ($TeO_3$, $TeO_4$, and $TeO_5$) are found in a single phase.[26]

Recent interest in new tellurite compounds in solid-state chemistry has mainly focused on mixed oxo-anions including $d^0$ transition metals such as $W^{6+}$ and $Mo^{6+}$ that are susceptible to second-order Jahn−Teller (SOJT) distortions, with a clear effort to design new noncentrosymmetric materials.[27−31] Similarly, the coordination geometry of $Mo^{6+}/W^{6+}$ cations are equally versatile, with four to six oxygen atoms being found to

**Received:** April 8, 2015
**Published:** May 28, 2015





DOI: 10.1021/acs.inorgchem.5b00789
*Inorg. Chem.* 2015, 54, 5981−5990

Table 1. Crystallographic Data of $ThWTe_2O_9$, $Th(WO_4)(TeO_3)$, $ThMoTe_2O_9$, and $Th_2(MoO_4)(TeO_3)_3$

| compound | $ThWTe_2O_9$ | $Th(WO_4)(TeO_3)$ | $ThMoTe_2O_9$ | $Th_2(MoO_4)(TeO_3)_3$ |
|---|---|---|---|---|
| mass | 815.08 | 655.48 | 727.18 | 1150.82 |
| space group | $I4_1/a$ | $P2_1/c$ | $C2/c$ | $P2_1/c$ |
| $a$ (Å) | 19.4824(16) | 4.1252(6) | 21.431(13) | 11.379(2) |
| $b$ (Å) | 19.4824(16) | 8.5122(14) | 7.046(3) | 7.1208(12) |
| $c$ (Å) | 7.7430(5) | 15.364(2) | 10.923(5) | 14.060(3) |
| $\beta$ (deg) | 90 | 92.599(12) | 110.33(4) | 90.60(2) |
| $V$ (Å$^3$) | 2939.0(5) | 538.95(14) | 1546.7(14) | 1139.2(4) |
| Z | 16 | 4 | 8 | 4 |
| $\lambda$ (Å) | 0.71073 | 0.71073 | 0.71073 | 0.71073 |
| $F$ (000) | 5440.0 | 1088.0 | 2464.0 | 1928.0 |
| $\mu$ (cm$^{-1}$) | 43.668 | 54.170 | 28.248 | 34.727 |
| $\rho_{calcd}$ (g cm$^{-3}$) | 7.368 | 8.078 | 6.246 | 6.710 |
| $R(F)$ for $F_0{}^2 > 2\sigma(F_0{}^2)^a$ | 0.0403 | 0.0419 | 0.0162 | 0.0243 |
| $wR_2$ $(F_0{}^2)^b$ | 0.0943 | 0.0872 | 0.0388 | 0.0469 |

$^aR(F) = \sum||F_0| - |F_c||/\sum|F_0|$ $^bR(F_0^2) = [\sum w(F_0^2 - F_c^2)^2/\sum w(F_0^4)^{1/2}$

form tetrahedral, square pyramidal, trigonal bipyramidal, or octahedral polyhedra. Considerable accomplishments have been gained in this regard in recent years. From these compounds, $BaTeM_2O_9$ (M = $Mo^{6+}$, $W^{6+}$),[28,29] $A_2TeM_3O_{12}$ (A = $NH^{4+}$, $Rb^+$, $Cs^+$; M = $Mo^{6+}$, $W^{6+}$),[32] and $(NH_4)_2Te_2WO_8$,[33] exhibit potential application in developing new devices in laser systems due to their satisfactory outcomes in the properties of piezoelectricity, pyroelectricity, and second-harmonic generation. The inclusion of rare earth metals into this system is of high interest due to the excellent luminescence and alexandrite effect of rare earth metals.[25] $Nd_2MoTe_3O_{12}$, for example, is considered as a possible luminescent candidate for 1.06 $\mu$m emission.[34]

However, comparing to a vast number of molybdate tellurites and tungstate tellurites containing alkali, alkaline earth, transition, and even rare earth metals, the study of actinide molybdate tellurites or tungstate tellurites remains in deep freeze, and until now there is no crystal structure reported in this family. Because of the versatility of coordination geometries of actinide elements,[35] it is expected that this family also possesses fascinating topological structural types. Recently, we have undertaken a systematic study on the synthesis and characterization of thorium compounds containing hexavalent cations ($Mo^{6+}$, $W^{6+}$, $Cr^{6+}$, $S^{6+}$, and $Se^{6+}$).[36,37] Our aim is to understand the synthetic and structural chemistry of these materials. As part of our ongoing research on actinide compounds containing hexavalent cations ($Mo^{6+}$, $W^{6+}$, $Cr^{6+}$, $S^{6+}$, and $Se^{6+}$), we have attempted the study of the thorium-molybdate/tungstate-tellurite system. Our efforts lead to four new compounds that simultaneously contain $MoO_4/WO_6$ and $Te^{4+}$ groups, namely, $ThWTe_2O_9$, $Th(WO_4)(TeO_3)$, $ThMoTe_2O_9$, and $Th_2(MoO_4)(TeO_3)_3$. In this report, we discuss the synthesis, crystal structures, thermal behaviors, and spectroscopic properties of these newly isolated compounds.

## EXPERIMENTAL SECTION

**2.1. Crystal Growth.** All the titled compounds were synthesized using the high-temperature solid-state method. All the chemicals were obtained from commercial sources as analytically pure and used without further purification. In order to decrease the synthesis temperature, excess $TeO_2$ and $WO_3$ were used for each crystal growth.

*$ThWTe_2O_9$.* $Th(NO_3)_4{\cdot}(H_2O)_5$ (50.0 mg, 0.0877 mmol), $TeO_2$ (42.0 mg, 0.263 mmol), and $WO_3$ (61.0 mg, 0.259 mmol) were weighed out. This results in a Th:Te:W ratio of 1:3:3. The mixture was fully ground and transferred into a 5 mL Pt crucible. After a holding time of 3 h at 780 °C for homogeneous melting, the furnace was cooled in two steps. First the temperature was gradually decreased by 5 °C/h to 250 °C, then to room temperature (RT) within 3 h. Brown colored crystals were found on the wall of the crucible and were hand-picked for further analyses. The yield cannot be calculated because the broken glassy pieces and crystals are indistinguishable.

*$Th(WO_4)(TeO_3)$.* $Th(NO_3)_4{\cdot}(H_2O)_5$ (50.0 mg, 0.0877 mmol), $TeO_2$ (28.0 mg, 0.175 mmol), $WO_3$ (81.3 mg, 0.351 mmol), and $LiNO_3$ (18.1 mg, 0.263 mmol) (molar ratio of Th:Te:W:Li = 1:2:4:3) were fully ground and were loaded into a 5 mL Pt crucible. The mixture was heated fast to 770 °C and held at this temperature for 3 h and then cooled to 250 °C by 5 °C/h followed by quenching. The resulting products in the form of yellow rectangular prisms were isolated and picked up for further analysis. Because of the difficulty to discern the crystals from broken glassy pieces, the yield cannot be obtained.

*$ThMoTe_2O_9$.* $Th(NO_3)_4{\cdot}(H_2O)_5$ (50 mg, 0.0877 mmol), $TeO_2$ (56.0 mg, 0.350 mmol), and $MoO_3$ (50.5 mg, 0.351 mmol) were fully ground and were loaded into a 5 mL Pt crucible. This leads to a Th:Te:Mo molar ratio of 1:4:4. The mixture was heated in a 5 mL Pt crucible up to 780 °C and then cooled to 50 °C with a cooling rate of 5 °C/h. The solid products consisting of $ThMoTe_2O_9$ crystals in the form of yellow rectangular prisms were isolated. Because of the difficultly to discern the crystals from broken glassy pieces, the yield cannot be obtained.

*$Th_2(MoO_4)(TeO_3)_3$.* $Th(NO_3)_4{\cdot}(H_2O)_5$ (50 mg, 0.0877 mmol), $TeO_2$ (28 mg, 0.175 mmol), and $MoO_3$ (50.5 mg, 0.351 mmol) were fully ground and loaded into a 5 mL Pt crucible. This results in a Th:Te:Mo molar ratio of 1:2:4. The mixture was placed into a furnace and heated to 750 °C. After 3 h, the reaction was cooled at a rate of 5 °C/h to room temperature. The reaction mixture contained auburn crystals which were found at the wall of the crucible. Because of the difficulty to discern the crystals from broken glass pieces, the yield cannot be obtained.

**2.2. Pure Phase Synthesis.** Pure polycrystalline powders of $ThWTe_2O_9$, $Th(WO_4)(TeO_3)$, $ThMoTe_2O_9$, and $Th_2(MoO_4)(TeO_3)_3$ were synthesized according to each corresponding stoichiometric ratio. Polycrystalline samples were prepared using the same reagents as those for the single crystal syntheses. The components were ground and placed into a furnace (CARBOLITE CWF 1300). In order to obtain the pure phase, the syntheses were carried out at various temperature points with steps of 20 °C starting from 400 °C until the compound melting point. After each temperature step, the purity of the reaction products was checked via X-ray powder diffraction by comparing the experimental and theoretical X-ray diffraction patterns. Finally, the pure phases of $ThWTe_2O_9$, $Th(WO_4)(TeO_3)$, $ThMoTe_2O_9$, and $Th_2(MoO_4)(TeO_3)_3$, were obtained around 660, 640, 640, and 580 °C, respectively. In this report, the pure phases were used in the thermal behavior experiments.



DOI: 10.1021/acs.inorgchem.5b00789
Inorg. Chem. 2015, 54, 5981−5990

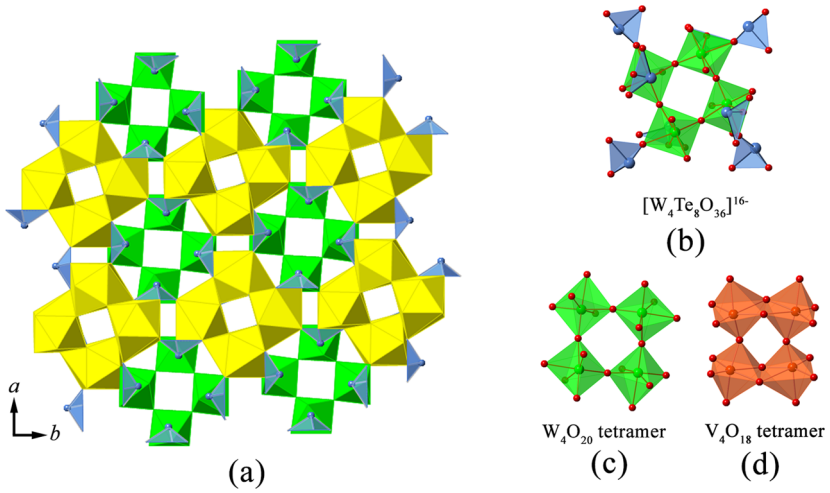


**Figure 1.** (a) Polyhedral presentation of the structure of $ThWTe_2O_9$. (b) The tungstotellurite cluster is constructed by corner-sharing of four $WO_6$ octahedra and eight $TeO_3$ trigonal pyramids. (c, d) Comparison of octahedral tetramers in $ThWTe_2O_9$ and $V_2O_3(XO_3)_2$ (X = Se, S), respectively. $WO_6$ polyhedra are shown in green, and $VO_6$ polyhedra are shown in orange. $ThO_9$ and $TeO_3$ polyhedra are shown in yellow and blue, respectively.

**2.3. Crystal Structure Studies.** The as-obtained crystals were selected for data collection. The crystals were mounted on glass fibers and optically aligned on an Agilent diffractometer (SuperNova, Dual Source). The data collection was done by a CCD area detector with a frame width of 0.2° and an exposure time of 20 s. The experiment was performed using a monochromatic Mo $K\alpha_{1,2}$ tube which has an incident wavelength of 0.71073 Å and runs at 50 kV and 0.8 mA providing a beam size of approximately 30 $\mu$m. The unit-cell dimensions for these crystals were refined using least-squares techniques against the positions of all measured reflections. More than a hemisphere of data were collected for each crystal and the three-dimensional data were reduced and filtered for statistical outliers using the standard *CrysAlis*$^{Pro}$ program. Data were corrected for Lorentz, polarization, absorption and background effects. The crystal structure determination and refinement were carried out using the *SHELXL-97* program.[38] The data and crystallographic information are given in Table 1. The structures were solved by direct methods and refined to $R_1$ = 0.040 for $ThWTe_2O_9$, $R_1$ = 0.042 for $Th(WO_4)(TeO_3)$, $R_1$ = 0.016 for $ThMoTe_2O_9$, and $R_1$ = 0.024 for $Th_2(MoO_4)(TeO_3)_3$, respectively.

**2.4. X-ray Powder Diffraction.** X-ray powder diffraction patterns for all powder samples were collected on a Bruker D4 Endeavor diffractometer, equipped with a Cu $K\bar{\alpha}$ ($\lambda$ = 1.54187 Å) tube and a one-dimensional silicon strip LynxEye detector (Bruker), using a voltage of 40 kV and an electric current of 40 mA (1.6 kW). Data were recorded in the range of $2\theta$ = 10−80° (total counting time =10 s/step with the step width of =0.2°). The aperture of the fixed divergence slit and the receiving slit were set to 0.2 mm and 8.0 mm, respectively. The X-ray powder diffraction patterns for $ThWTe_2O_9$, $Th(WO_4)(TeO_3)$, $ThMoTe_2O_9$ and $Th_2(MoO_4)(TeO_3)_3$ are provided in the Supporting Information (Figure S1).

**2.5. Scanning Electron Microscopy/Energy-Dispersive X-ray Spectroscopy (SEM/EDS).** Scanning electron microscopy images and energy-dispersive X-ray spectroscopy (SEM/EDS) data were collected on a FEI Quanta 200F Environmental scanning electron microscope. The instrument is equipped with an Apollo Silicon Drift Detector (SDD) from EDAX. The measurements were carried out in a low-vacuum mode at 60 Pa (30 kV, spot size 4 $\mu$m, working distance 10 mm). The EDS results shown in the Supporting Information (Figure S2 and Table S1), are well in agreement with the chemical compositions for all four thorium compounds.

**2.6. DSC and TG Analysis.** The thermal behavior of the dried pure polycrystalline powders was studied from room-temperature up to 1200 °C by differential scanning calorimetry analysis (DSC) and thermogravimetry (TG) in air. Using a Netzsch STA 449C Jupiter apparatus, 20 mg of sample was each loaded into a platinum crucible which was closed with a platinum cover. During the measurements a constant air flow of around 20−30 mL/min at a heating rate of 10 °C/min was applied.

**2.7. Raman Spectroscopy.** Utilizing a Peltier cooled multichannel CCD detector, the unpolarized Raman spectra were recorded with a Horiba LabRAM HR spectrometer. All the samples were in the form of single crystals. An objective with a 50× magnification was linked to the spectrometer, allowing the analysis of samples as small as 2 $\mu$m in diameter. The incident radiation was produced by a He−Ne laser at a power of 17 mW ($\lambda$ = 632.81 nm). The focal length of the spectrometer was 800 mm and a 1800 gr/mm grating was used. The spectral resolution was around 1 $cm^{-1}$ with a slit of 100 $\mu$m. The Raman spectroscopic investigation for all samples was executed at room temperature in the range of 100−1050 $cm^{-1}$.

**2.8. Bond-Valence Analysis.** Bond-valence sums (BVS) for all atom positions in the four thorium tellurium compounds were calculated. The bond-valence parameters for Th(IV)-O, W(VI)-O, Mo(VI)-O and Te(IV)-O were used according to Brese and O'Keefe.[39] The BVS for all atoms fit well with their expected formal valence.

## 3. RESULTS AND DISCUSSION

**Synthesis.** Due to the unstable thermal behavior of tellurium compounds, the corresponding crystals can be obtained by either reducing the growth temperature or performing the reaction under sealed conditions.[40−43] In fact, a large number of molybdate/tungstate tellurites have been successfully synthesized by the solid-state method using a $MoO_3$ or $TeO_2$ flux, which allows the crystals to grow at a relative low temperature (below 800 °C).[30,44] These significant achievements encouraged us to take such a method into first consideration. During our experiment, we found that a high $TeO_2$ ratio always led to high viscosity of the melted mixture promoting glass formation, while a low ratio could result in low yields or in phases not involving the Te element. The results of different synthesis experiments demonstrate that these mixed oxo-anion crystals are preferable to be grown with Mo(W):Te ratios from 1:1 to 2:1.

It is noteworthy that the formation of these four compounds is stoichiometrically sensitive, which implies that different structural building blocks can be formed by changing the molar ratio of raw materials. We found that $Th(WO_4)(TeO_3)$ and $Th_2(MoO_4)(TeO_3)_3$, where all oxo-anions are separated from each other, were favored in the reactions which had a slightly


DOI: 10.1021/acs.inorgchem.5b00789
*Inorg. Chem.* 2015, 54, 5981−5990

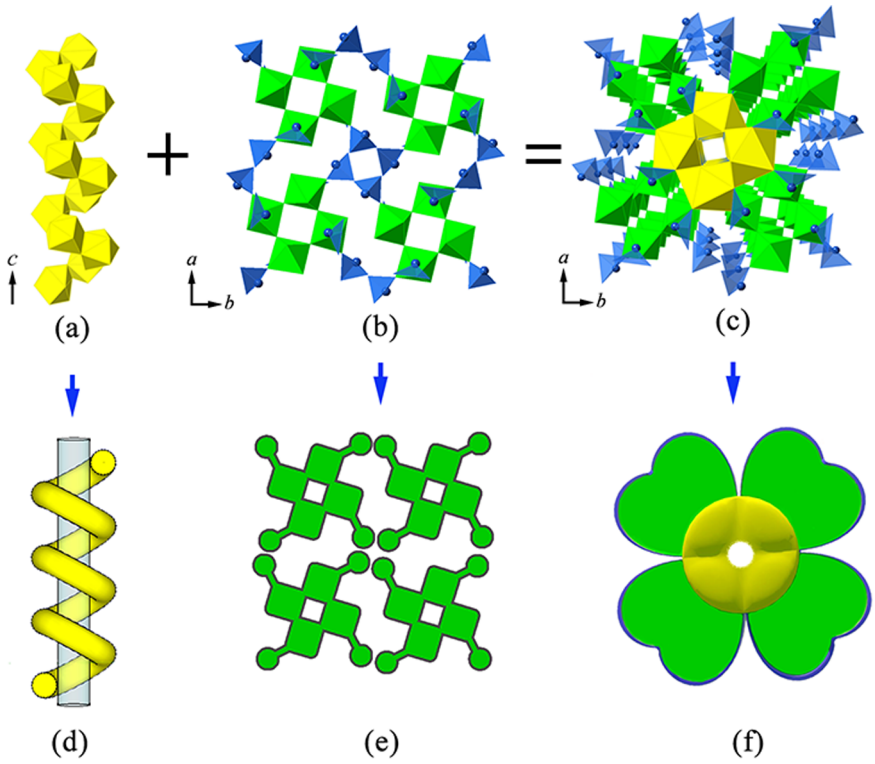


**Figure 2.** Representation of $ThWTe_2O_9$ composed by the helical thorium chains and tungstotellurite clusters. (a, d) The thorium chains in the structure of $ThWTe_2O_9$ constructed by edge-sharing of $ThO_9$ polyhedra along the *c*-axis. (b, e) Four tungstotellurite clusters in a spiral fashion. (c, f) Due to the 4-fold screw axis, when viewing along the *c*-axis, the resulting structural fragment has a cross-section similar to four-leafed clovers.

lower Mo(W)/Te ratio. By comparison, the other two compounds $ThWTe_2O_9$ and $ThMoTe_2O_9$ which contain the Te−O−W or Te−O−Mo linkages can be isolated from the reactions of a higher Mo(W)/Te ratio.

**Structures and Topology.** *$ThWTe_2O_9$.* The $ThWTe_2O_9$ is built from a complex 3D framework composed of $ThO_9$, $TeO_3$ and $WO_6$ polyhedra with the space group $I4_1/a$ (Figure 1a). It contains one symmetrically independent Th site, which is nine-coordinated by O atoms from two neighboring Th, six Te, and two W cations, creating an environment around the center thorium atom that can be best described as a monocapped square antiprism. The Th−O bond distances fall in the range of 2.27(1)−2.64(1) Å. There are two Te sites and each is coordinated by three O atoms in a trigonal pyramidal geometry. For Te(1), the Te−O bond distances range from 1.83(1) Å to 1.94(1) Å, while the $Te(2)O_3$ shows slightly less perturbation with the variation in Te−O bonds in the range from 1.86(1) Å to 1.94(1) Å. These two $TeO_3$ groups exhibit quite similar coordination features; that is, all of them are pentadentate and each $TeO_3$ polyhedron forms one bidentate chelation with one Th atom and also bridges with two other Th and one W atoms. Finally, the only octahedral $WO_6$ site is significantly distorted. The distortion is manifested as a movement toward the face of the octahedron along the local $C_3$ direction, producing three short (1.74(1)−1.80(1) Å) and three long W−O bonds (2.05(1)−2.12(1) Å). This out-of-center distortion is common for octahedrally coordinated $W^{6+}$ cations attributable to the second-order Jahn−Teller (SOJT) distortions.[41,45,46] The O−W−O bond angles are also observed to deviate from the ideal octahedral geometry, i.e., being in the range of 77.7(4)° to 103.6(5)° for cis O−W−O bonds and from 161.4(4)° to 168.3(4)° for trans ones. As being noted in many molybdenum/tungsten selenite/tellurite compounds, the $MO_6$ (M = W, Mo) octahedra are distorted more from the O atoms bonded to the $Te^{4+}$, owing to the lone pair electrons.[47] The bond valence calculation based on the Th−O, Te−O, and W−O bond distances were calculated to be 4.03, 3.61−3.80, and 6.31 v.u. respectively, and they are consistent with the ideal values asked for Th(IV), Te(IV), and W(VI).

The octahedral tetramer, as shown in Figure 1c, formed by four $WO_6$ octahedra interlinking via equatorial corners, is remarkable as it has not been found in other actinide tungstate compounds. Similar four-membered rings with equal topological configuration can be observed in the structure of $V_2O_3(XO_3)_2$ (X = Se, S) (Figure 1d).[48] However, in the latter structure, such tetramer is composed of two pairs of edge-shared octahedra by connecting octahedral corners. The $W_4O_{20}$ tetramer is connected by four $Te(1)O_3$ and four $Te(2)O_3$ to result in a tungstotellurite cluster $[W_4Te_8O_{36}]^{16-}$ with complex topology (Figure 1b). It is noteworthy to mention that the term "tungstotellurite" is typically used to name phases where tungstate groups are directly linked with tellurite groups. In contrast, compounds consist of isolated tungstate and tellurite groups are denoted as "tungstate tellurite".[49,50] Due to containing clusters of $[W_4Te_8O_{36}]^{16-}$, here the $ThWTe_2O_9$ becomes the first tugnstotellurite compound among all actinide families.

The most extraordinary aspect of the structure of $ThWTe_2O_9$ lies at the helical Th chains constructed by edge-sharing of neighboring $ThO_9$ polyhedra along the *c*-axis (Figure 2a,d). The Th−Th bond distance of 4.12(0) Å is in good agreement with those observed in other reported thorium tungstate compounds.[51] To the best of our knowledge, no solid-state compounds containing such a helical Th structural config-


DOI: 10.1021/acs.inorgchem.5b00789
*Inorg. Chem.* 2015, 54, 5981−5990

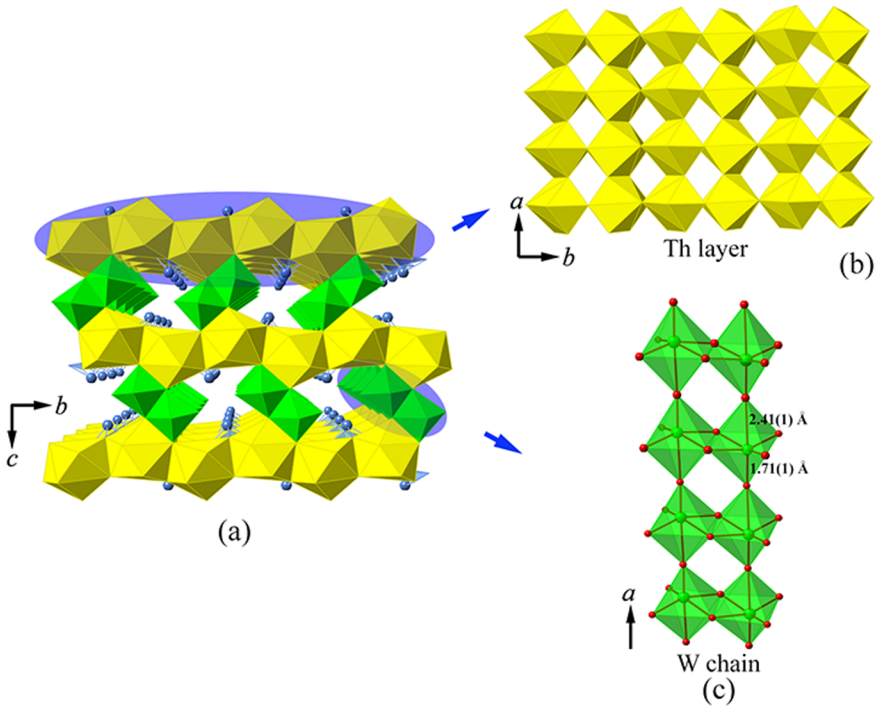


**Figure 3.** (a) View of the structure of $Th(WO_4)(TeO_3)$ containing Th sheets and W chains projected along the [100] direction. (b) Th layers. (c) W chains with alternating short and long W−O bond distances for two apical trans-oxygens.

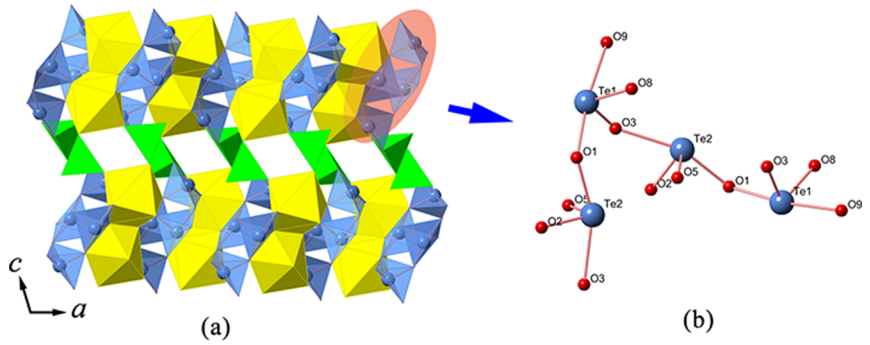


**Figure 4.** (a) Projection of the structure of $ThMoTe_2O_9$ along the *b*-axis. (b) $[Te_2O_5]^{2-}$ infinite chains. $MoO_4$ polyhedra are shown in green, $ThO_9$ polyhedra are shown in yellow, and $TeO_3$ polyhedra are shown in blue.

uration have been reported. Each Th chain lies on a 4-fold screw axis, as required by the space group $I4_1/a$, and is further linked with four tungstotellurite clusters in a spiral fashion to complete the $ThWTe_2O_9$ framework, as shown in Figure 2b,e. Due to the 4-fold screw axis, when viewed along the *c*-axis, the resulting structural fragment has a cross-section of four-leafed clovers (see Figure 2c,f). In $ThWTe_2O_9$, each $WO_6$ octahedron in the $W_4O_{20}$ tetramer shares one edge with a $ThO_9$ polyhedron within one thorium chain and a corner with another $ThO_9$ polyhedron in a neighboring thorium chain. As in the case of $TeO_3$ groups, the $Te(2)O_3$ polydedra are bidentate and monodentate between every fourth $ThO_9$ polyhedron along the chain length, respectively, whereas the $Te(1)O_3$ polydedra which are not involved in the thorium chain play a role in fusing adjacent thorium chains. The lone pairs, for the Te(1) atoms, which are arranged in alternate order along the spiral direction, are oriented parallel to the (001) plane, whereas for the $Te(2)O_3$ trigonal pyramids, all the lone pairs point approximately into the [001] direction.

*$Th(WO_4)(TeO_3)$.* The structure of $Th(WO_4)(TeO_3)$ crystallizes in the space group $P2_1/c$. It is built upon $ThO_9$ monocapped square antiprisms, $TeO_4$ polyhedra and $WO_6$ octahedra. The $ThO_9$ monocapped square antiprisms are bound by common edges to create chains extending along the [010] direction. These Th chains are found to be most similar to those in $ThTe_2O_6$ where the Th chains are connected by $TeO_3$ and $TeO_4$ polyhedra.[52] In $Th(WO_4)(TeO_3)$, however, the thorium chains are not interlinked by $TeO_3$ trigonal pyramids, but rather they are fused together along the [100] direction, creating 2D Th sheets which are inlaid with $TeO_3$ polyhedra (Figure 3a,b). The Th−O bond distance, ranging from 2.36(1) to 2.73(1) Å with an average value of 2.48 Å, fits well with the typical nine-coordinated thorium in other compounds.[3,53] The only Te site in $TeO_4$ polyhedral configuration, with BVS result of 4.04 v.u., is bidentatedly chelated by four Th atoms with the lone pairs located on the opposite sides of the sheets. The bond distances of Te−O range from 1.88(1) Å to 2.45(1) Å with an average value of 2.03 Å. In the case of W sites, two $WO_6$ octahedra are bound



DOI: 10.1021/acs.inorgchem.5b00789
*Inorg. Chem.* 2015, 54, 5981−5990

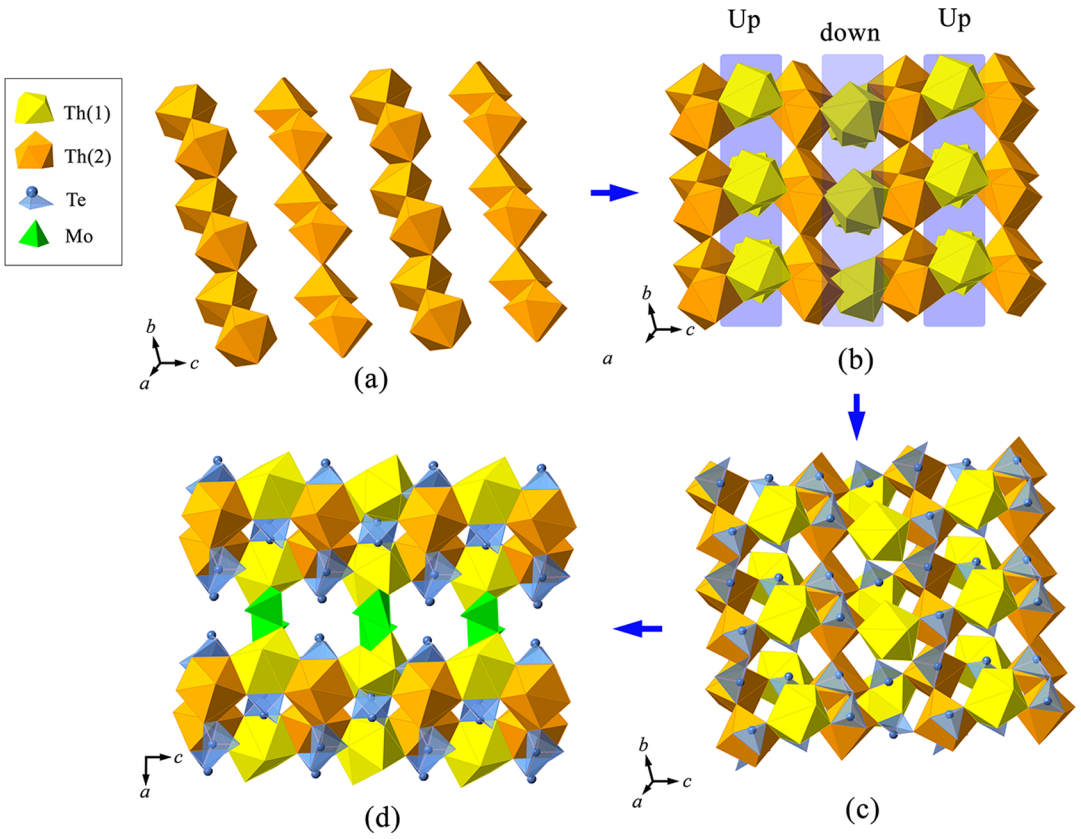


**Figure 5.** Proposed construction procedure of the structure of $Th_2(MoO_4)(TeO_3)_3$. (a) The $Th(2)O_8$ square antiprisms share two common edges to result in chains which are one polyhedron wide and propagate along the [010] direction. (b) These chains are interconnected into a zigzag thorium sheet with Th(1) polyhedra located by the sequence of an "up and down" manner between the adjacent $Th(2)O_8$ chains. (c) The gaps within the thorium sheets are filled with $TeO_3$ and $TeO_4$ polyhedra, leading to a thorium tellurite sheet $[Th_2(TeO_3)_3]^{2+}$ parallel to the (100) plane. (d) The $[Th_2(TeO_3)_3]^{2+}$ sheets are further linked into a 3D framework with the help of $MoO_4$ tetrahedra, completing the structure of $Th_2(MoO_4)(TeO_3)_3$.

together by a common edge, forming a $W_2O_{10}$ dimer. If viewing along the [100] direction, one can observe such $W_2O_{10}$ dimers are interconnected in a corner-sharing manner, shown in Figure 3c. This results in an alternating short (1.71(1) Å) and long (2.41(1) Å) W−O bond distance for two apical O atoms in the trans configuration. The remaining W−O bond distances involved in the equatorial plane range from 1.78(1) to 2.08(1) Å. Similar tungsten chains have also been observed in a series of lanthanide compounds $Ln(WO_4)_2$ (A = K and Cs; Ln = La, Gd, Lu, and Y).[54,55] Finally, the above-mentioned Th−Te sheets are connected together with these tungsten chains in between, resulting in a multilayer-sandwich framework of $Th(WO_4)$-$(TeO_3)$. The joining of the Th−Te sheets with tungsten chains also leads to channels filled with lone pairs of electrons propagating in the [100] direction.

*$ThMoTe_2O_9$.* $ThMoTe_2O_9$, forming in the *C*2/*c* space group, features a 3D framework structural type constructed by the linkages of $ThO_9$, $MoO_4$ and $TeO_4$ polyhedra (Figure 4a). The only Th site in $ThMoTe_2O_9$ is again coordinated with nine O atoms to form a distorted tricapped trigonal prismatic coordination geometry. The bond distances for Th−O are in the range of 2.295(3) Å to 2.876(4) Å with the average value of around 2.497 Å, and are comparable with other reported thorium compounds.[16,56] Two $ThO_9$ polyhedra are interconnected to a $Th_2O_{16}$ dimer by sharing a common edge. In $ThMoTe_2O_9$ two $TeO_4$ polyhedra, $Te(1)O_4$ and $Te(2)O_4$, are interlinked via O(3) and O(1) atoms with their lone pairs orientated roughly in opposite directions, producing $[Te_2O_5]^{2-}$ infinite chains along the *c*-axis, presented in Figure 4b. The Te−O bond distances, between 1.842(3) Å and 2.395 (3) Å, fall in the typical range required for $TeO_4$ geometry.[57] It is noted that such tellurium chains have not been observed in telluride compounds containing actinide elements. The Te−Te distance within the chain, 3.645(3) Å, is comparable with that in other telluride compounds.[58] The $Th_2O_{16}$ dimers are incorporated into the above tellurium chains to generate $[Th(Te_2O_5)]^{2+}$ thorium tellurite sheets extending parallel to the (001) plane. Due to the lone pairs, the thorium tellurite sheets themselves are puckered, and they are further interconnected by $MoO_4$ tetrahedra, resulting in the formation of a 3D framework. The Mo−O bond distance for Mo−O−Te, is relatively short, 1.738(3) Å, compared to those involved in the $ThO_9$ connection (between 1.759(3) Å and 1.813 (4) Å).

*$Th_2(MoO_4)(TeO_3)_3$.* $Th_2(MoO_4)(TeO_3)_3$ crystallizes in the $P2_1/c$ space group with two crystallographically different Th sites, three different Te sites and one Mo site. It is a 3D framework where the Th polyhedra are interconnected by $TeO_3$, $TeO_4$ and $MoO_4$ polyhedra. The Th(1) cations are nine-coordinated with O atoms, featuring a monocapped square antiprismatic coordination geometry, whereas Th(2) cations form distorted square antiprisms by linking with eight O atoms. It is to be noted, that up to now, among all the inorganic thorium molybdates available in literature, only two compounds, orthorhombic-$Th(MoO_4)_2$[59] and $Cs_2Th_3(MoO_4)_7$,[53]


DOI: 10.1021/acs.inorgchem.5b00789
*Inorg. Chem.* 2015, 54, 5981−5990

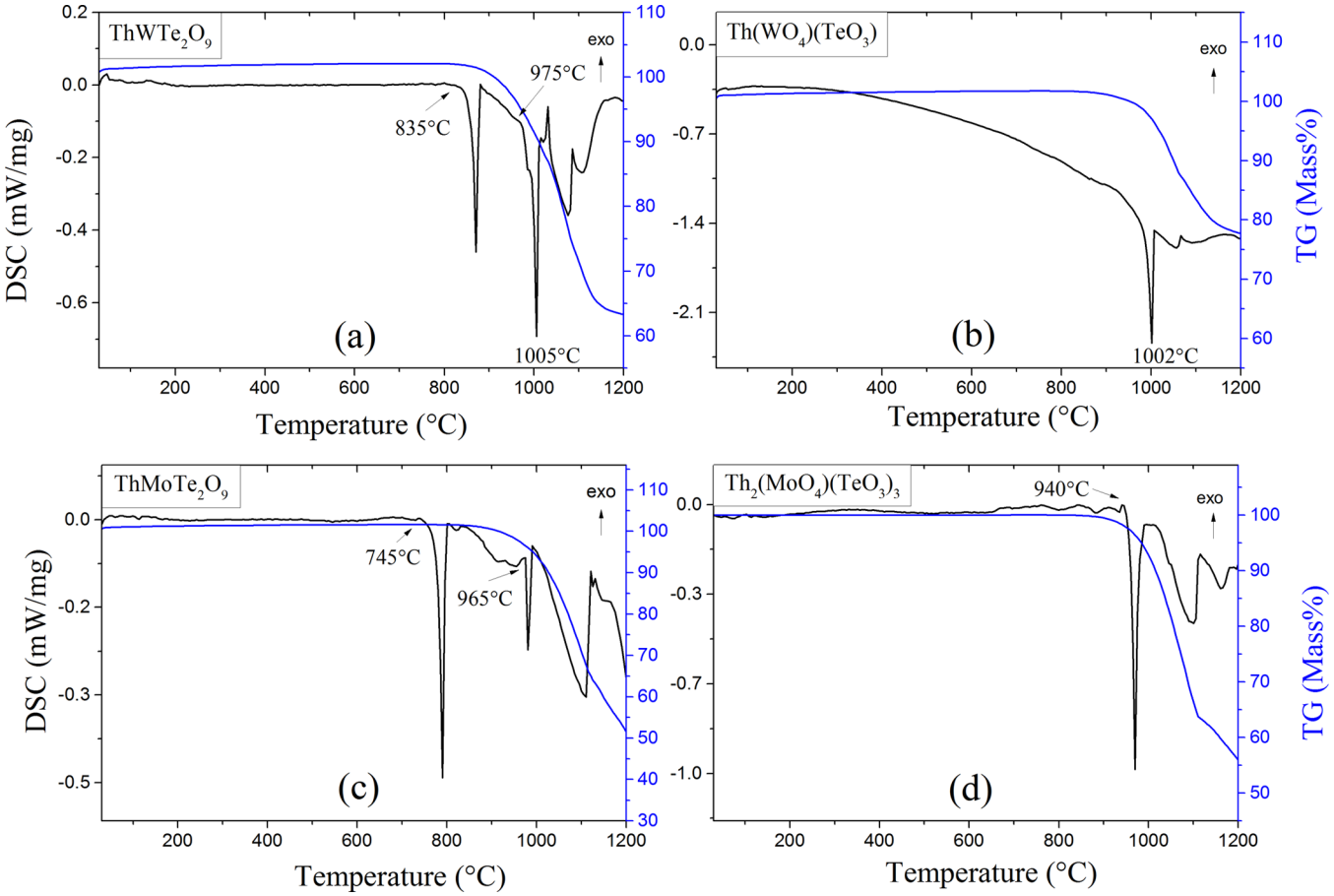


**Figure 6.** DSC and TG diagram of (a) $ThWTe_2O_9$, (b) $Th(WO_4)(TeO_3)$, (c) $ThMoTe_2O_9$, and (d) $Th_2(MoO_4)(TeO_3)_3$, respectively.

are found to contain more than one kind of thorium−oxygen polyhedral. The Th−O bond distances vary from 2.357(5) to 2.842(6) Å with the average value of 2.46 Å, which is comparable with that found in $ThMoTe_2O_9$. The coordination geometry around Te(1) is disphenoid ($TeO_4$), while Te(2) and Te(3) can be demonstrated as trigonal pyramids ($TeO_3$) with lone pairs occupying the pyramidal sites. The bond valence calculations for Te(1) and Te(2) are 3.95 and 3.82 v.u. respectively, confirming that all the Te atoms are in the oxidation state of +4. The Te−O bond distances are in the range of 1.864(5) to 2.275(5) Å. As in most thorium molybdate compounds, the Mo atoms are in a slightly distorted tetrahedral geometry with O−Mo(1)−O angles ranging from 102.6(3)° to 113.0(3)°. More specifically, the shortest Mo(1)−O(13) bond, 1.733(6) Å, is terminal while the three long Mo(1)−O bonds from 1.770(6) to 1.796(6) Å are further linked to Th(1) cations.

As shown in Figure 5a, the adjacent $Th(2)O_8$ square antiprisms in $Th_2(MoO_4)(TeO_3)_3$ share two common edges to result in chains which are one polyhedron wide and run along the [010] direction. These chains are interconnected into a zigzag thorium sheet by sharing edges with $Th(1)O_9$ monocapped square antiprisms which are located by the sequence of "up and down" between the neighboring $Th(2)O_8$ chains (Figure 5b). The resulting thorium sheet displays a rather loose configuration, and the space of which is filled with $TeO_3$ and $TeO_4$ polyhedra, leading to a thorium tellurite sheet $[Th_2(TeO_3)_3]^{2+}$ parallel to the (100) plane (Figure 5c). Unlike the compound of $ThMoTe_2O_9$ where the Te atoms are constructed into infinite chains, in $Th_2(MoO_4)(TeO_3)_3$ they are isolated or constructed into dimers. As can be seen from Figure 5, among the thorium tellurite sheet, the $Te(3)O_3$ and $Te(1)O_4$ polyhedra share one common O atom to form a $[Te_2O_6]^{4-}$ dimer. The resulting $[Te_2O_6]^{4-}$ dimer chelates bidentately with one Th(2) atom and also bridges with one Th(1) and another two Th(2). The $Te(2)O_3$ polyhedra are found to bidentately chelate with one Th(1) atom and bridge with two Th(2) and another Th(1) atom. The $[Th_2(TeO_3)_3]^{2+}$ sheets are further linked into a 3D framework with the help of $MoO_4$ tetrahedra which serve as a role of interlayer linkers. Each $MoO_4$ linker shares three of its corner O atoms with surrounding $Th(1)O_8$ polyhedra. Note that the adjacent $MoO_4$ tetrahedra are orientated in an opposite direction from each other by the sequence of the nonshared O corners. The unshared O atoms of these $MoO_4$ tetrahedra, with alternative [001] and [00$\bar{1}$] orientations, are located parallel to the direction of thorium tellurite sheets. The 3D framework, from Figure 5d, possesses small voids observed in the [010] direction which are filled with the lone pairs of the $Te(3)O_3$ polyhedra.

The connection manner for $MoO_4$ tetrahedra in $ThMoTe_2O_9$ is different from that of $Th_2(MoO_4)(TeO_3)_3$. In the latter, each $MoO_4$ tetrahedron shares only 3 O atoms hooking on adjacent thorium tellurite sheets, while there is no terminal O atom for $MoO_4$ tetrahedra in the former structure. Each $MoO_4$ tetrahedron in $ThMoTe_2O_9$ shares two of its corners with two $ThO_9$ tricapped trigonal prisms from one $[Th(Te_2O_5)]^{2+}$ sheet, one corner with one $ThO_9$ polyhedron from the opposite thorium tellurite sheet and another corner with a


DOI: 10.1021/acs.inorgchem.5b00789
Inorg. Chem. 2015, 54, 5981−5990

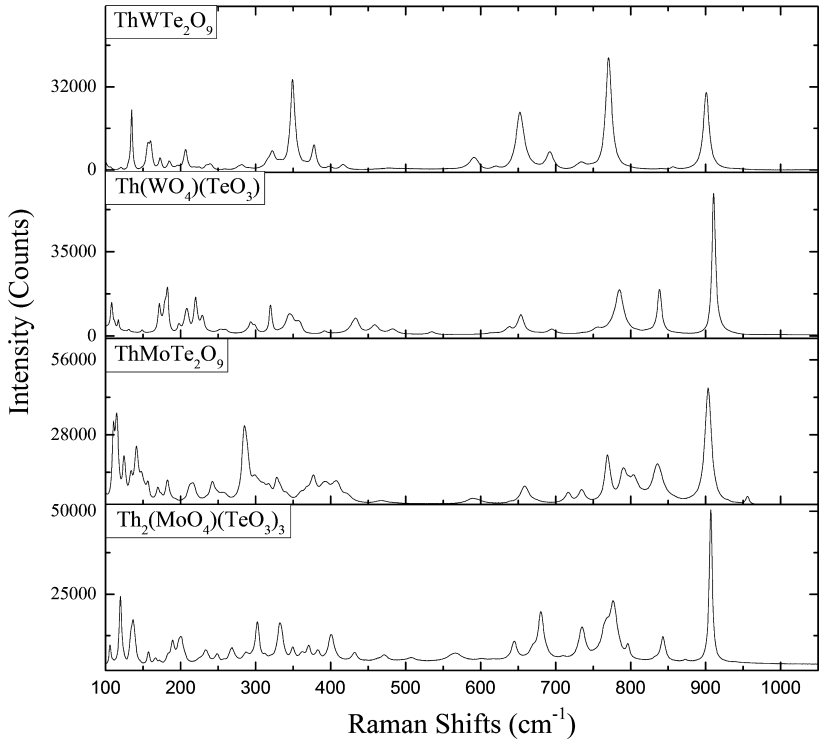


**Figure 7.** Raman spectra of $ThWTe_2O_9$, $Th(WO_4)(TeO_3)$, $ThMoTe_2O_9$, and $Th_2(MoO_4)(TeO_3)_3$, respectively.

$Te(2)O_4$ tetrahedron. Another difference is the connection manner of the hexavalent oxo-anions. In $Th_2(MoO_4)(TeO_3)_3$ all $MoO_4$ tetrahedra are completely separated from tellurium units, whereas the $MoO_4$ octahedra are linked directly with $TeO_4$ units to give rise to a Mo−O−Te linkage. As a result, $ThMoTe_2O_9$ can be named as "molybdotellurite", while $Th_2(MoO_4)(TeO_3)_3$ should be called "molybdate tellurite".[49,50]

It can clearly be seen that the tungstotellurite $ThWTe_2O_9$ and molybdotellurite $ThMoTe_2O_9$ are based on the same chemical stoichiometric ratio (Th:W/Mo:Te = 1:1:2). However, there is a remarkable contrast between their structures. In this case, one can note how critical the oxo-ainons affect the formation of crystal structures. In $ThWTe_2O_9$, tungstotellurites fragments are constructed from corner-sharing $WO_6$ octahedra and $TeO_3$ units which are further connected by a spiral Th chain to from complex four-leafed clover fragments. Whereas, $ThMoTe_2O_9$ is built from $Th(Te_2O_5)^{2+}$ thorium tellurite sheets which are further interconnected by $MoO_4$ tetrahedra.

**3.1. Thermal Behavior.** DSC and TG measurements were performed simultaneously for as-synthesized pure polycrystalline samples from room temperature to 1200 °C. The DSC curves for $ThWTe_2O_9$ and $ThMoTe_2O_9$ are quite similar. Both samples have two sharp endothermic peaks. In the case of $ThWTe_2O_9$ (Figure 6a), the first peak with onset at around 835 °C exhibits a characteristic of large mass loss, which indicates the sample is melting and decomposing. The major phase that is indicated by powder XRD for the decomposing products is $ThW_2O_8$. A considerable amount of the material decomposes continuously when further heated to nearly 1000 °C, which is accompanied by the second endothermic DSC effect starting at 975(7) °C. Two endothermic peaks were observed during the heating of $ThMoTe_2O_9$, with onset at 745(7) and 965(7) °C, respectively, shown in Figure 6c. The higher temperature peak, without a doubt, associated with a solid−liquid transformation behavior. What is interesting is the first peak ranging from 745(7) to 805(7) °C for $ThMoTe_2O_9$. Since there is no appreciable variation of weight observed in this region, it is possible to make a hypothesis of solid−solid phase transition. However, considering the thermal instability of most molybdate tellurite compounds at high temperature (>800 °C),[60,61] this assumption is speculative. From the powder XRD measurements, which were collected after heating the polycrystalline samples of $ThMoTe_2O_9$ slightly above the first peak for 5 h, one was able to identify the orthorhombic-$ThMo_2O_8$ and $MoTe_2O_7$ as the dominant phases. This means, that the corresponding peak should be assigned to the sample decomposition. Only one endothermic peak appears during the heating of $Th(WO_4)(TeO_3)$, with maxima at 1002(3)°C (Figure 6b), which is related to the melting point, as evidenced by powder XRD technique after heating the corresponding sample slightly across this temperature peak. The thermal behavior for $Th_2(MoO_4)(TeO_3)_3$ presents a similar pattern, with only one melting peak starting at around 940 °C (Figure 6d).

**3.2. Raman Spectroscopy.** The Raman spectra of all the above-described thorium compounds are presented in Figure 7. Nevertheless, very few vibrational spectra of thorium contained molybdates/tungstates or tellurites have been published. The ideal $MoO_4^{2-}$ has the $T_d$ symmetry with the 4 normal motions being assigned as $A_1(\nu_1)$; $E(\nu_2)$; $F_1(rot)$, $F_2(trans, \nu_3, \nu_4)$ where $A_1$, $E$ and $F_2$ are Raman permitted while $F_2$ is IR active. The $\nu_1$, $\nu_2$, $\nu_3$, and $\nu_4$ modes are denoted as nondegenerated symmetric stretching, doubly degenerated symmetric bending, triply degenerated asymmetric stretching, and asymmetric bending vibrations, respectively. The stretching vibrations of $\nu_1$ and $\nu_3$ in free $MoO_4^{2-}$ are placed in the region of 700−1000 $cm^{-1}$, while the bending vibrations ($\nu_2$ and $\nu_4$) are situated in the scope of 300−500 $cm^{-1}$. For $WO_6$ octahedra, the $\nu_1$ mode is always observed as the strongest Raman line around 800−950 $cm^{-1}$.[62]



DOI: 10.1021/acs.inorgchem.5b00789
Inorg. Chem. 2015, 54, 5981−5990

In comparison, the $\nu_2$ mode of $WO_6$ is less clear in the spectra and often gives rise to very weak signals in broad wavenumber range from 500 to 770 $cm^{-1}$. The ideal $TeO_3^{2-}$ trigonal pyramid has a $C_{3v}$ symmetry consisting of four vibrational frequencies: two nondegenerate $\nu_1$ and $\nu_2$ modes and the other two doubly degenerate $\nu_3$ and $\nu_4$ modes.[63,64]

Because of the complexity of our reported compounds, here we assign only selected frequencies based on a comparison of literature data. For all the vibrational data, the high frequency bands ranging from 600 to 950 $cm^{-1}$ are characterized by the presence of individual bands, among which are rather loose bands with high intensity. These bands can be attributed to the stretching vibrations of Te−O and Mo(W)-O, primarily associated with the motions of O atoms.[65,66] The lower range of the spectra, from 200 to 450 $cm^{-1}$, are characterized by broad overlapping bands with lower intensity, which may correspond to one or a conjunction of the vibrations of Te−O and Mo(W)−O, because this is an overlapping region for these vibrations.[67] The spectral range below 200 $cm^{-1}$ is dominated by the presence of partially overlapping bands, mainly contributed from the motions of the "lattice skeleton".[68−70] For $Th(WO_4)(TeO_3)$, the highest peak of 910(1) $cm^{-1}$ can be unambiguously attributed to the symmetric stretching mode ($\nu_1$) of W−O. However, this peak is shifted to 901(1) $cm^{-1}$ and becomes the second highest peak for $ThWTe_2O_9$. A close resemblance between the Raman spectra of $ThMoTe_2O_9$ and $Th_2(MoO_4)(TeO_3)_3$ can be detected. Similarly, the highest peak around 903(1) and 906(1) $cm^{-1}$ for $ThMoTe_2O_9$ and $Th_2(MoO_4)(TeO_3)_3$, respectively, can be attributed to the stretching mode ($\nu_1$) of Mo−O.[69−71]

## 4. CONCLUSION

We demonstrate that tetravalent chalcogenes can be combined with oxo-anions of hexavalent transition elements within the actinide bearing compounds. Structural study of obtained materials reveals the influence of tetravalent tellurium cations on the crystal chemistry of thorium molybdates or tungstates. All the as-synthesized compounds are built from thorium polyhedra bridged through tetrahedral $MoO_4$ (or octahedral $WO_6$) and tellurium units ($TeO_3$ or $TeO_4$). One exception, the $Th_2(MoO_4)(TeO_3)_3$, contains both $ThO_9$ and $ThO_8$ polyhedra, all other phases are composed exclusively by $ThO_9$ polyhedra. The $ThWTe_2O_9$ and $ThMoTe_2O_9$ have the same stoichiometric composition, but crystallize in utterly different structures. The structure of $ThWTe_2O_9$ can be seen as based on complex four-leafed clover fragments constructed by a center spiral Th chain interlinked with four tungstotellurite clusters around its corners. $ThMoTe_2O_9$, however, is built from $Th(Te_2O_5)^{2+}$ thorium tellurite sheets which are further interconnected by $MoO_4$ tetrahedra.

The structures of titled thorium compounds containing tetravalent molybdate/tungstate oxo-anions are fundamentally different from those observed in $ThM_2O_8$; M = Mo or W. The presence of tetravalent Te in these four compounds substantially complicates the original Th−O−Mo(W) uniformity, making the corresponding structural linkages rather complex. Moreover, in order to sustain charge neutrality, the replacement of $Mo(VI)O_4/W(VI)O_6$ polyhedra by $Te(IV)O_x$ ($x$ = 3, 4, 5) oxo-anions results in a low amount of hexavalent cations (Mo/W), which considerably increases the Th/Mo(W) ratio and further makes the structures of thorium molybdates/tungstates more complex. In conclusion, the basic thorium molybdate/tungstate tellurites shown in this report may help guide future research on the 5f-element chemistry, as it is expected that more and more compounds with new structures and interesting properties will be further prepared by introducing the alkali or alkaline earth metals into this family.

## ■ ASSOCIATED CONTENT

### Supporting Information

EDS analysis, atomic ratios, and CIF files. The Supporting Information is available free of charge on the ACS Publications website at DOI: 10.1021/acs.inorgchem.5b00789.

## ■ AUTHOR INFORMATION

### Corresponding Author

*E-mail: e.alekseev@fz-juelich.de.

### Notes

The authors declare no competing financial interest.

## ■ ACKNOWLEDGMENTS

We are grateful to the Helmholtz Association for the funding within VH-NG-815 grant.

## ■ REFERENCES

(1) Wu, S.; Wang, S.; Diwu, J.; Depmeier, W.; Malcherek, T.; Alekseev, E. V.; Albrecht-Schmitt, T. E. *Chem. Commun. (Cambridge, U. K.)* **2012**, *48*, 2334−2336.
(2) Wu, S.; Wang, S.; Polinski, M.; Beermann, O.; Kegler, P.; Malcherek, T.; Holzheid, A.; Depmeier, W.; Bosbach, D.; Abrecht-Schmitt, T. E.; Alekseev, E. V. *Inorg. Chem.* **2013**, *52*, 5110−5118.
(3) Yu, N.; Klepov, V. V.; Kegler, P.; Bosbach, D.; Albrecht-Schmitt, T. E.; Alekseev, E. V. *Inorg. Chem.* **2014**, *53*, 8194−8196.
(4) Yu, N.; Klepov, V. V.; Modolo, G.; Bosbach, D.; Suleimanov, E. V.; Gesing, T. M.; Robben, L.; Alekseev, E. V. *Inorg. Chem.* **2014**, *53*, 11231−11241.
(5) Burns, P. C. *Can. Mineral.* **2005**, *43*, 1839−1894.
(6) Krivovichev, S.; Burns, P.; Tananaev, I. *Structural chemistry of inorganic actinide compounds*; Elsevier: Amsterdam, 2006.
(7) Daly, S. R.; Piccoli, P. M. B.; Schultz, A. J.; Todorova, T. K.; Gagliardi, L.; Girolami, G. S. *Angew. Chem., Int. Ed.* **2010**, *49*, 3379−3381.
(8) Wang, G.; Zhang, L.; Lin, Z.; Wang, G. *J. Alloys Compd.* **2010**, *489*, 293−296.
(9) Wang, S.; Yu, P.; Purse, B. A.; Orta, M. J.; Diwu, J.; Casey, W. H.; Phillips, B. L.; Alekseev, E. V.; Depmeier, W.; Hobbs, D. T.; Albrecht-Schmitt, T. E. *Adv. Funct. Mater.* **2012**, *22*, 2241−2250.
(10) Yu, P.; Wang, S.; Alekseev, E. V.; Depmeier, W.; Hobbs, D. T.; Albrecht-Schmitt, T. E.; Phillips, B. L.; Casey, W. H. *Angew. Chem., Int. Ed.* **2010**, *49*, 5975−5977.
(11) Dacheux, N.; Thomas, A.; Chassigneux, B.; PichotI, E.; Brandel, V.; Genet, M. In Study of Th4 (PO4) 4 P2O7 and Solid Solutions With U (IV), Np (IV) and Pu (IV): Synthesis, Characterization, Sintering and Leaching Tests. *MRS Proceedings, 1999*; Cambridge University Press: New York, 1999; p 85.
(12) Dacheux, N.; Podor, R.; Chassigneux, B.; Brandel, V.; Genet, M. *J. Alloys Compd.* **1998**, *271−273*, 236−239.
(13) Salvadó, M. A.; Pertierra, P.; Bortun, A. I.; Trobajo, C.; García, J. R. *Inorg. Chem.* **2005**, *44*, 3512−3517.
(14) Nelson, A.-G. D.; Bray, T. H.; Stanley, F. A.; Albrecht-Schmitt, T. E. *Inorg. Chem.* **2009**, *48*, 4530−4535.
(15) Huyghe, M.; Lee, M. R.; Quarton, M.; Robert, F. *Acta Crystallogr., Sect. C* **1991**, *47*, 1797−1799.
(16) Huyghe, M.; Lee, M. R.; Quarton, M.; Robert, F. *Acta Crystallogr., Sect. C* **1991**, *47*, 244−246.
(17) Woodward, J. D.; Almond, P. M.; Albrecht-Schmitt, T. E. *Acta Crystallogr. Sect. E* **2005**, *61*, i58−i60.
(18) Galy, J.; Meunier, G. *Acta Crystallogr. B* **1971**, *27*, 608.


DOI: 10.1021/acs.inorgchem.5b00789
*Inorg. Chem.* 2015, 54, 5981−5990

(19) Swihart, G. H.; Gupta, P. K. S.; Schlemper, E. O.; Back, M. E.; Gaines, R. V. *Am. Mineral.* **1993**, *78*, 835.
(20) Meunier, G.; Galy, J. *Acta Crystallogr. B* **1973**, *29*, 1251.
(21) Kim, H.; Cho, Y.; Yun, H.; Do, J. *Z. Anorg. Allg. Chem.* **2007**, *633*, 473−477.
(22) Kim, M. K.; Kim, S. H.; Chang, H. Y.; Halasyamani, P. S.; Ok, K. M. *Inorg. Chem.* **2010**, *49*, 7028−7034.
(23) Li, P.-X.; Zhang, S.-Y.; Mao, J.-G. *Dalton Trans.* **2010**, *39*, 11560−11567.
(24) Vidyavathy; Vidyasagar, K. *Inorg. Chem.* **1998**, *37*, 4764−4774.
(25) Lin, J.; Diefenbach, K.; Cross, J. N.; Babo, J.-M.; Albrecht-Schmitt, T. E. *Inorg. Chem.* **2013**, *52*, 13278−13281.
(26) Kim, J.-H.; Halasyamani, P. S. *J. Solid State Chem.* **2008**, *181*, 2108−2112.
(27) Goodey, J.; Broussard, J.; Halasyamani, P. S. *Chem. Mater.* **2002**, *14*, 3174−3180.
(28) Ra, H. S.; Ok, K. M.; Halasyamani, P. S. *J. Am. Chem. Soc.* **2003**, *125*, 7764−7765.
(29) Yu, Q.; Gao, Z.; Zhang, S.; Zhang, W.; Wang, S.; Tao, X. *J. Appl. Phys.* **2012**, *111*, 013506−013506.
(30) Zhang, J.; Zhang, Z.; Sun, Y.; Zhang, C.; Tao, X. *CrystEngComm* **2011**, *13*, 6985−6990.
(31) Zhang, J.; Zhang, Z.; Zhang, W.; Zheng, Q.; Sun, Y.; Zhang, C.; Tao, X. *Chem. Mater.* **2011**, *23*, 3752−3761.
(32) Feng, X.; Zhang, J.; Gao, Z.; Zhang, S.; Sun, Y.; Tao, X. *Appl. Phys. Lett.* **2014**, *104*, 081912−081912.
(33) Kim, J.-H.; Baek, J.; Halasyamani, P. S. *Chem. Mater.* **2007**, *19*, 5637−5641.
(34) Shen, Y.-L.; Jiang, H.-L.; Xu, J.; Mao, J.-G.; Cheah, K. W. *Inorg. Chem.* **2005**, *44*, 9314−9321.
(35) Burns, P. C.; Ewing, R. C.; Hawthorne, F. C. *Can. Mineral.* **1997**, *35*, 1551−1570.
(36) Xiao, B.; Langer, E.; Dellen, J.; Schlenz, H.; Bosbach, D.; Suleimanov, E. V.; Alekseev, E. V. *Inorg. Chem.* **2015**, *54*, 3022−3030.
(37) Xiao, B.; Gesing, T. M.; Robben, L.; Bosbach, D.; Alekseev, E. V. *Chem.—Eur. J.* **2015**, *21*, 7746−7754.
(38) Sheldrick, G. *Acta Crystallogr., Sect. A* **2008**, *64*, 112−122.
(39) Brese, N. E.; O'Keeffe, M. *Acta Crystallogr., Sect. B* **1991**, *47*, 192−197.
(40) Chi, E. O.; Ok, K. M.; Porter, Y.; Halasyamani, P. S. *Chem. Mater.* **2006**, *18*, 2070−2074.
(41) Goodey, J.; Broussard, J.; Halasyamani, P. S. *Chem. Mater.* **2002**, *14*, 3174−3180.
(42) Guesdon, A.; Raveau, B. *Chem. Mater.* **2000**, *12*, 2239−2243.
(43) Kim, J.-H.; Baek, J.; Halasyamani, P. S. *Chem. Mater.* **2007**, *19*, 5637−5641.
(44) Zhang, W.; Li, F.; Kim, S.-H.; Halasyamani, P. S. *Cryst. Growth Des.* **2010**, *10*, 4091−4095.
(45) Nguyen, S. D.; Halasyamani, P. S. *Inorg. Chem.* **2012**, *51*, 9529−9538.
(46) Goodey, J.; Min Ok, K.; Broussard, J.; Hofmann, C.; Escobedo, F. V.; Halasyamani, P. S. *J. Solid State Chem.* **2003**, *175*, 3−12.
(47) Zhang, S.-Y.; Mao, J.-G. *Inorg. Chem.* **2011**, *50*, 4934−4943.
(48) Tyutyunnik, A. P.; Krasil'nikov, V. N.; Zubkov, V. G.; Perelyaeva, L. A.; Baklanova, I. V. *Russ. J. Inorg. Chem.* **2010**, *55*, 501−507.
(49) Ewald, B.; Huang, Y.-X.; Kniep, R. *Z. Anorg. Allg. Chem.* **2007**, *633*, 1517−1540.
(50) Kniep, R.; Engelhardt, H.; Hauf, C. *Chem. Mater.* **1998**, *10*, 2930−2934.
(51) Bang Jin, G.; Soderholm, L. *J. Solid State Chem.* **2011**, *184*, 337−342.
(52) López, M. L.; Veiga, M. L.; Jerez, A.; Pico, C. *J. Alloy Comp.* **1991**, *175*, 235−241.
(53) Xiao, B.; Gesing, T. M.; Kegler, P.; Modolo, G.; Bosbach, D.; Schlenz, H.; Suleimanov, E. V.; Alekseev, E. V. *Inorg. Chem.* **2014**, *53*, 3088−3098.
(54) Torardi, C. C.; Page, C.; Brixner, L. H.; Blasse, G.; Dirksen, G. J. *J. Solid State Chem.* **1987**, *69*, 171−178.
(55) Gallucci, E.; Goutaudier, C.; Cohen-Adad, M. T.; Mentzen, B. F.; Hansen, T. *J. Alloys Compd.* **2000**, *306*, 227−234.
(56) Albrecht, A. J.; Sigmon, G. E.; Moore-Shay, L.; Wei, R.; Dawes, C.; Szymanowski, J.; Burns, P. C. *J. Solid State Chem.* **2011**, *184*, 1591−1597.
(57) Weil, M. *Z. Anorg. Allg. Chem.* **2014**, *640*, 128−135.
(58) Lin, J.; Diwu, J.; Cross, J. N.; Villa, E. M.; Albrecht-Schmitt, T. E. *Inorg. Chem.* **2012**, *51*, 10083−10085.
(59) Cremers, T. L.; Eller, P. G.; Penneman, R. A. *Acta Crystallogr., Sect. C* **1983**, *39*, 1165−1167.
(60) Bart, J. C. J.; Petrini, G.; Giordano, N. *Z. Anorg. Allg. Chem.* **1975**, *412*, 258−270.
(61) Petrini, G.; Bart, J. C. J. *Z. Anorg. Allg. Chem.* **1981**, *474*, 229−232.
(62) Mączka, M.; Tomaszewski, P.; Stępień-Damm, J.; Majchrowski, A.; Macalik, L.; Hanuza, J. *J. Solid State Chem.* **2004**, *177*, 3595−3602.
(63) Dussack, L. L.; Harrison, W. T. A.; Jacobson, A. J. *Mater. Res. Bull.* **1996**, *31*, 249−255.
(64) Ratheesh, R.; Suresh, G.; Bushiri, M. J.; Nayar, V. U. *Spectrochim. Acta, Part A* **1995**, *51*, 1509−1515.
(65) Domoratskii, K. V.; Pastukhov, V. I.; Kudzin, A. Y.; Sadovskaya, L. Y.; Rizak, V. M.; Stefanovich, V. A. *Phys. Solid State* **2000**, *42*, 1443−1446.
(66) Mirgorodsky, A. P.; Merle-Méjean, T.; Thomas, P.; Champarnaud-Mesjard, J. C.; Frit, B. *J. Phys. Chem. Solids* **2002**, *63*, 545−554.
(67) Vidyavathy; Vidyasagar, K. *Inorg. Chem.* **1998**, *37*, 4764−4774.
(68) Hanuza, J.; Mączka, M.; van der Maas, J. H. *J. Mol. Struct.* **1995**, *348*, 349−352.
(69) Hermanowicz, K.; Mączka, M.; Dereń, P. J.; Hanuza, J.; Stręk, W.; Drulis, H. *J. Lumin.* **2000**, *92*, 151−159.
(70) Mahadevan Pillai, V. P.; Pradeep, T.; Bushiri, M. J.; Jayasree, R. S.; Nayar, V. U. *Spectrochim. Acta, Part A* **1997**, *53*, 867−876.
(71) Mączka, M.; Paraguassu, W.; Souza Filho, A. G.; Freire, P. T. C.; Melo, F. E. A.; Mendes Filho, J.; Hanuza, J. *J. Raman Spectrosc.* **2005**, *36*, 56−62.


DOI: 10.1021/acs.inorgchem.5b00789
*Inorg. Chem.* 2015, 54, 5981−5990